ACCEPTED VERSION

Deyu Bao, Linsen Huang, Yingjie Gao, Kenneth Davey, Yao Zheng, Shi-Zhang Qiao
Dynamic Creation of a Local Acid-like Environment for Hydrogen Evolution Reaction in Natural Seawater
Journal of the American Chemical Society, 2024; 146(50):34711-34719

This document is the Accepted Manuscript version of a Published Work that appeared in final form in Journal of the American Chemical Society, copyright © 2024 American Chemical Society after peer review and technical editing by the publisher. To access the final edited and published work see https://doi.org/10.1021/jacs.4c13036

PERMISSIONS

https://pubs.acs.org/page/authors/sharing.htm#post-accepted

Posting Accepted Manuscripts and Published Articles on Websites and Repositories

Authors may post the Accepted Manuscript or Published Article on personal websites, publicly accessible repositories, or private collaboration groups under these conditions:

- Posting is mandated by an author's funder, institution, or employer.
- If posting is required sooner than 12 months after publication, authors may seek a waiver or choose immediate availability via an Article Development Charge or ACS Open Access option.
- If allowed after 12 months, the Accepted Manuscript may be posted with this notice: *"This document is the Accepted Manuscript version of a Published Article that appeared in final form in [Journal Title], copyright © [insert copyright notice]. To access the final published article, see ACS Articles on Request."*

Posting must be non-commercial and comply with ACS Ethical Guidelines to Publication of Chemical Research. A digital file of the Published Article may only be made publicly available via an ACS Open Access option. Authors may share links to the Published Article on the ACS website using the ACS Articles on Request link.

24 February 2026

http://hdl.handle.net/2440/144055

Dynamic Creation of a Local Acid-Like Environment for Hydrogen Evolution Reaction in Natural Seawater

Deyu Bao, Linsen Huang, Yingjie Gao, Kenneth Davey, Yao Zheng*, Shi-Zhang Qiao*

School of Chemical Engineering, The University of Adelaide, Adelaide, SA 5005, Australia.

Keywords: local acid-like environment; hydrogen evolution reaction (HER); hydrogen tungsten bronze; natural seawater electrolysis

ABSTRACT: Electrolysis of natural seawater driven by renewable energy is practically attractive for green hydrogen production. However, because precipitation initiated by an increase in local pH near to the cathode deactivates catalysts or blocks electrolyzer channels, limited catalysts are capable of operating with untreated, natural seawater (*viz.* pH 8.2 to 8.3 and *ca.* 35 g salts L^{-1}); most are used in strongly alkaline or acidic seawater. Here we report a new natural seawater electrolysis cathode with precipitation-suppression *via* a Pt/WO_2 catalyst to create a dynamically local acid-like environment. The *in-situ* formed hydrogen tungsten bronze (H_xWO_y) phase *via* continuous hydrogen insertion from water acts as a proton reservoir. As a result, dynamically stored protons create a local acid-like environment near the Pt active sites. We evidence that this tailored acid-like environment boosts hydrogen evolution reaction (HER) in natural seawater splitting and neutralizes generated OH^- species to restrict precipitation formations. Consequently, a long-term stability of > 500 h at 100 mA cm^{-2} was exhibited in direct seawater electrolysis.

1. INTRODUCTION

Electrolysis of natural seawater (*viz.* pH 8.2 to 8.3 and *ca.* 35 g salts L^{-1}) for hydrogen (H_2) production is practically attractive to reduce use of freshwater.[1-3] However, H_2 production based on direct seawater electrolysis is technically difficult, because dissolved ions (Na^+, Cl^-, Mg^{2+}, Ca^{2+}, SO_4^{2-}, etc.) in natural seawater can initiate deactivation of catalysts, electrodes and membranes.[4-6] Currently reported research focuses on improving existing technologies for seawater splitting, which includes proton exchange membrane (PEM) electrolyzers and alkaline water electrolyzers (AWE) that feeds high purity water *via* pre-treatment seawater by external purification or desalination systems.[7] However, pre-treatment of seawater or external alkali/acid addition contributes to costs and energy input.[8, 9] Direct seawater electrolysis is more economic for large-scale H_2 production.[10] There are however few reported investigations on untreated seawater electrolysis. The practical difficulty for operation is that the pH at the cathode surface rapidly increases with current density during hydrogen evolution reaction (HER) in natural seawater without sufficient buffers capacity, leading to *in-situ* precipitation formation near the cathode surface including, $Mg(OH)_2$ and $Ca(OH)_2$ when local pH value is ≥ ~9.5. These precipitates readily block the cathode surface, deactivate catalysts and degrade HER performance.[7, 11-14]

To obviate these practical difficulties, a catalyst with precipitation-suppression at the cathode is needed for natural seawater electrolysis. To date however, most reported investigations have focused on alkaline seawater electrolysis because this external alkali additive can remove dissolved Mg^{2+} and Ca^{2+} ions in an additional pre-treatment step. The cathode reaction can therefore be considered a conventional alkaline HER in freshwater, with the only difficulty to engineer an anodic catalyst to obviate chloride impact. Catalyst design has focused therefore on anode design for alkaline seawater electrolysis, with reported catalysts targeted on HER in natural seawater being limited. So far, several reports have established that the local environmental regulation on the catalyst surface affects kinetics and selectivity of reactions.[15, 16] Based on this, it is reported that adjusting local environment at the catalyst surface allows direct seawater electrolysis.[17, 18] A strongly local alkaline microenvironment build was able to inhibit precipitation formation at cathode, but introducing an ex-situ Lewis acid layer (Cr_2O_3 or V_2O_3) on catalysts may challenge by insufficient durability.

It was hypothesized therefore that creation of a local acid-like environment on a catalyst surface could obviate precipitation formation. This is because acidic media excludes insoluble precipitates generation and boosts HER performance with supplied protons.[19, 20] Reported methods for local acid-like environments for boosting HER in neutral and basic freshwater systems address improving electrocatalytic active site for promoting HER kinetics.[21-23] Externally introducing a local acid-like environment on these catalysts is likely unsustainable during adsorption of reactants and desorption of products on active sites, however, *in-situ* creation of a local acid-like environment over a catalyst would afford a dynamic HER during natural seawater electrolysis to, importantly, negate instability of catalyst and precipitates formation.

Here we report a new dynamic-regulation method to obviate precipitation in untreated seawater electrolysis.

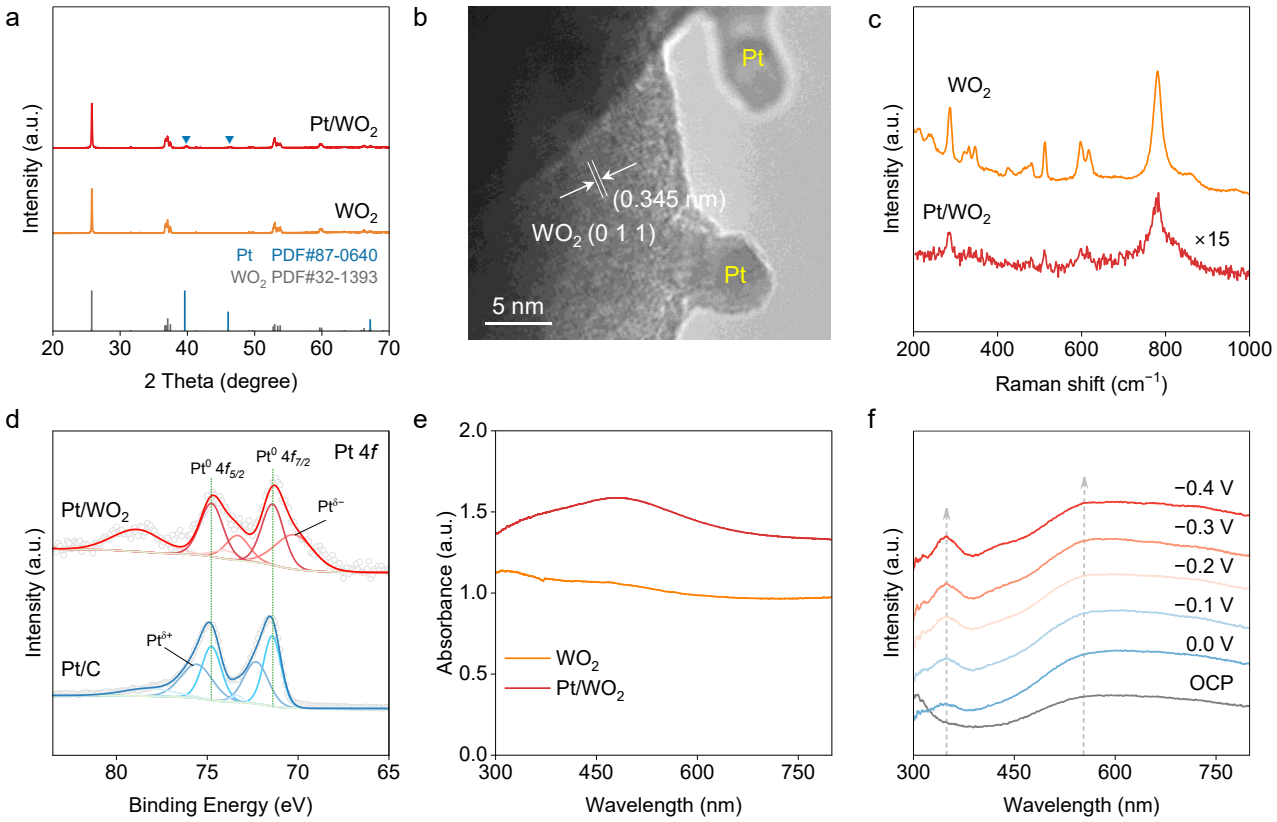


Figure 1. Characterization of catalysts. (a) XRD patterns for WO_2 and Pt/WO_2. (b) High-resolution TEM image for Pt/WO_2. (c) Raman spectra for WO_2 and Pt/WO_2. (d) High-resolution XPS spectra for Pt 4*f* for Pt/WO_2 and commercial Pt/C. (e) UV-vis absorption spectra for WO_2 and Pt/WO_2. (f) In-situ UV-vis absorption spectra for Pt/WO_2 at varying potential.

We demonstrate a designed Pt/WO_2 catalyst with a local acid-like environment that boosts HER and suppresses precipitation by limiting the increase of local pH at the cathode. Because of the reversible behavior of hydrogen insertion/extraction for WO_2, *in-situ* formed hydrogen tungsten bronze (H_xWO_y) acts as a proton 'sponge', stores H^+ and supplies to the active sites of Pt during HER. We establish that this dynamic process accumulates H_3O^+ on Pt surface to create a local acid-like environment. We confirm the local pH of Pt/WO_2 remained < 9.5 whilst the value was multiplying dramatically to 12 for benchmark Pt/C in natural seawater (collected at Henley Beach, South Australia, −34.92029, 138.49442 with pH ~ 8.3). Significantly, we show a long-term stability of > 500 h at 100 mA cm^{-2} in natural seawater electrolysis.

2. RESULTS AND DISCUSSION

2.1. Characterization of Catalysts. Pt was deposited on WO_2 *via* a hydrothermal and thermal decomposition method (*see* Methods for details). X-ray diffraction (XRD) findings confirmed a pure monoclinic phase of WO_2 (PDF#32–1393) and the presence of Pt species (PDF#87–0640, **Figure 1a** and S1, Table S1). Scanning electron microscopy (SEM) images and energy-dispersive X-ray spectroscopy (EDS) elemental mapping analysis confirmed the Pt, W and O were homogeneously dispersed throughout nanoparticle-like Pt/WO_2 cluster (Figure S2 and S3). Transmission electron microscopy (TEM) images showed Pt nanoparticles *ca.* 5 nm in size are loaded on WO_2 skeleton with a lattice parameter of 0.345 nm for WO_2 (**Figure 1b** and S4). In Raman spectroscopy (**Figure 1c**), the electronic interaction between Pt and WO_2 makes the vibrational peak for Pt/WO_2 weaker compared with pure WO_2, establishing that Pt nanoparticles are anchored on WO_2.[24] X-ray photoelectron spectroscopy (XPS) findings confirmed Pt^0 states existed in Pt/WO_2 (**Figure 1d**).[25] Notably, Pt in Pt/WO_2 catalyst were in $Pt^{\delta-}$ states, in contrast to standard Pt/C ($Pt^{\delta+}$ states).[26] This finding confirmed the electrons transfer between Pt and WO_2 to electron-enrich around Pt atoms in Pt/WO_2.[21, 27-30] As shown in Figure S5, Pt L_3-edge X-ray absorption near-edge spectroscopy (XANES) for catalysts further confirmed the presence of $Pt^{\delta-}$ states, which was reflected in the slightly lower intensity of white-line peak for Pt/WO_2 than that for Pt foil.[21, 31] Furthermore, Fourier-transformed Pt L_3-edge extended X-ray absorption fine structure (EXAFS) signal for Pt/WO_2 revealed an obvious scattering path corresponding to Pt-Pt bond at 2.63 Å, indicating the formation of Pt nanoparticles with Pt^0 metallic states,[32, 33] which aligns with XPS results for Pt 4*f*. Additionally, compared with WO_2, a greater binding energy for the lattice oxygen and W^{4+} 4*f* states for Pt/WO_2 confirmed this migration (Figure S6). More oxygen vacancies (O_{Vs}) in Pt/WO_2 were readily identifiable than that for WO_2 (Figure S6b), therefore it exhibited significantly greater absorbance than that for WO_2 (**Figure 1e**).[23, 34, 35] *In-situ* ultraviolet-visible (UV-vis) absorption spectroscopy confirmed two peaks at 350 and 554 nm boosted with cathodal potential, evidencing that more oxygen

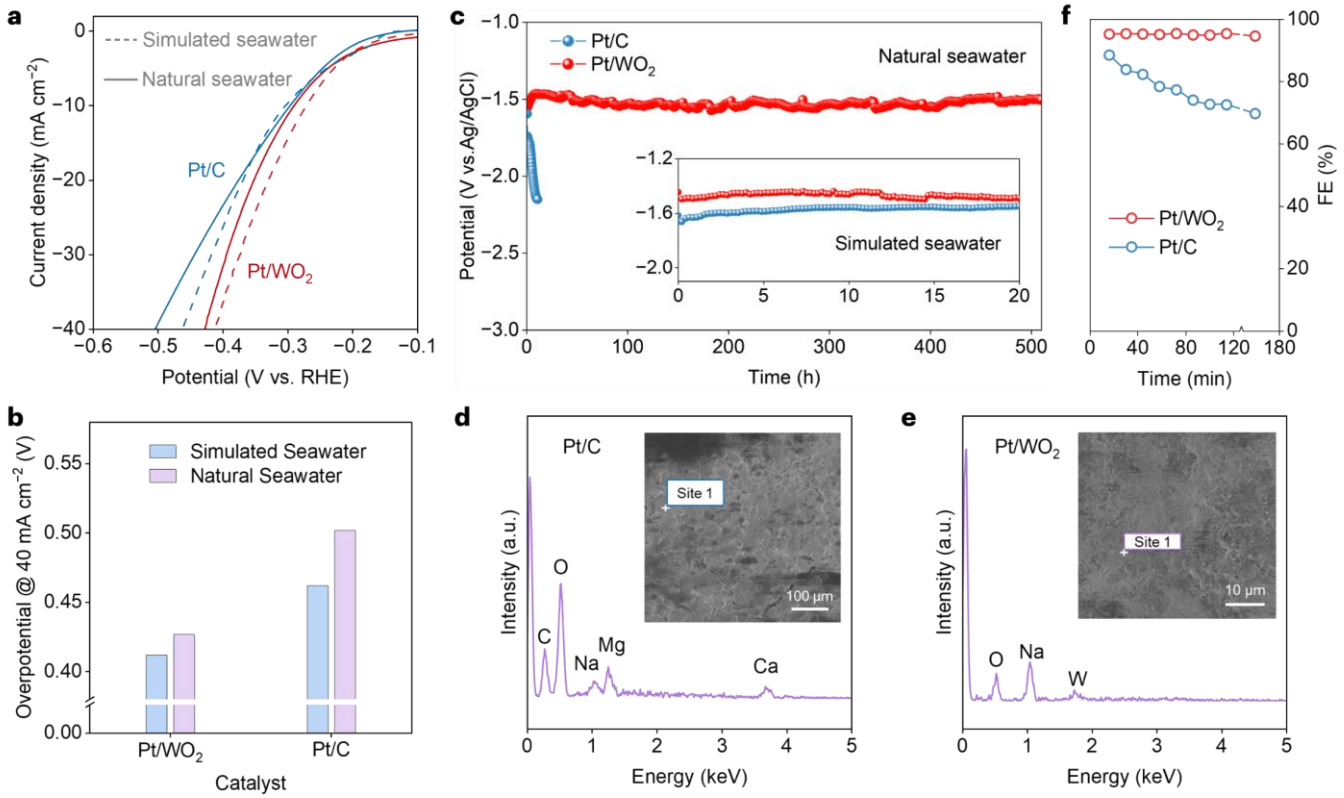


Figure 2. HER performance for catalysts in simulated and natural seawater. (a) LSV curves for Pt/WO_2 and Pt/C in Ar-saturated simulated seawater (dashed line) and natural seawater (solid line). (b) Comparison of overpotential for Pt/WO_2 and Pt/C at current density 40 mA cm^{-2} in different electrolyte. (c) Stability testing at 100 mA cm^{-2} over Pt/WO_2 and Pt/C in natural seawater under Ar (insert: simulated seawater). EDS for (d) Pt/C and (e) Pt/WO_2 following stability testing, insets correspond to SEM images of cathodes. (f) FE for hydrogen over Pt/C and Pt/WO_2 within 3 h.

vacancies generated during electrocatalysis favor charge storage (**Figure 1f**).[36-38]

2.2. Electrocatalytic HER Performance in Natural Seawater. HER performance of catalysts in a three-electrode electrochemical cell in natural seawater (without any treatment) was determined. Of these, 10 wt.% Pt/WO_2 catalyst exhibited greatest HER performance, requiring overpotential of just 290 and 420 mV to reach a current density of 10 and 40 mA cm^{-2}, respectively, values significantly better than for Pt/C (**Figure 2a, b** and S7-S9).A similar performance for the catalysts was exhibited in simulated seawater, *viz*. 0.6 M sodium chloride without Ca^{2+}/Mg^{2+} and pH controlled to 8.3 *via* addition of KOH (1.0 M). Stability tests with Pt/WO_2 and Pt/C at 100 mA cm^{-2} in simulated seawater were determined for a continuous 20 h, in which both catalysts remained stable without evidence of activity decline (**Figure 2c insert**). In natural seawater, Pt/C exhibited an apparent attenuation of activity within a few hours, whereas Pt/WO_2 exhibited a long-term durability > 500 h of continuous operation without meaningful activity decay (**Figure 2c**). To establish the difference between Pt/C and Pt/WO_2, the cathodes following a long-term stability test in natural seawater were compared. XRD and EDS findings of post-reaction electrodes showed that Ca^{2+} and Mg^{2+} was concentrated on the Pt/C catalyst surface, together with formation of significant precipitates, undetectable to XRD diffraction peaks of carbon paper (**Figure 2d** and S10). However, Pt/WO_2 remained exposed on the carbon paper (**Figure 2e**).

It was concluded therefore the disparity in stability between Pt/C and Pt/WO_2 is because of active sites of Pt/C poisoned by precipitation due to pH increase near them. This difference causes ion 'poisoning' and active sites decay of Pt/C.[39] Hydrogen production for Pt/C and Pt/WO_2 in natural seawater at 100 mA cm^{-2} within 3 h was determined. Mean Faradaic efficiency (FE) for hydrogen was 95% for Pt/WO_2 whilst for Pt/C it decreased from 88 to *ca*. 69% (**Figure 2f** and S11). These findings agree well with those reported for Pt/C in natural seawater from cations (Ca^{2+}/Mg^{2+}) poisoning (precipitates).[19]

2.3. Identifying the Local-acid Environment. To establish difference in precipitation formation between Pt/C and Pt/WO_2 in natural seawater, the local pH on catalysts surface was determined using a rotating ring-disk electrode (RRDE; Figure S12).[23, 40, 41] As is seen in **Figure 3a**, the local pH of the Pt/C surface increases from 8.2 to 12 together with the potential input from 0 to −0.5 V_{RHE}, *in-situ* accompanying by precipitates formation near the cathode when local pH is > 9.5. In contrast, a sluggish increase in local pH for Pt/WO_2 was exhibited, with corresponding pH values < 9.5 in the same range of potential, preliminarily suggesting that less, local OH^- was generated on the Pt/WO_2 surface (**Figure 3b**, S13). With increase of Pt in Pt/WO_2, at the same potential (−0.4 V_{RHE}), the local pH

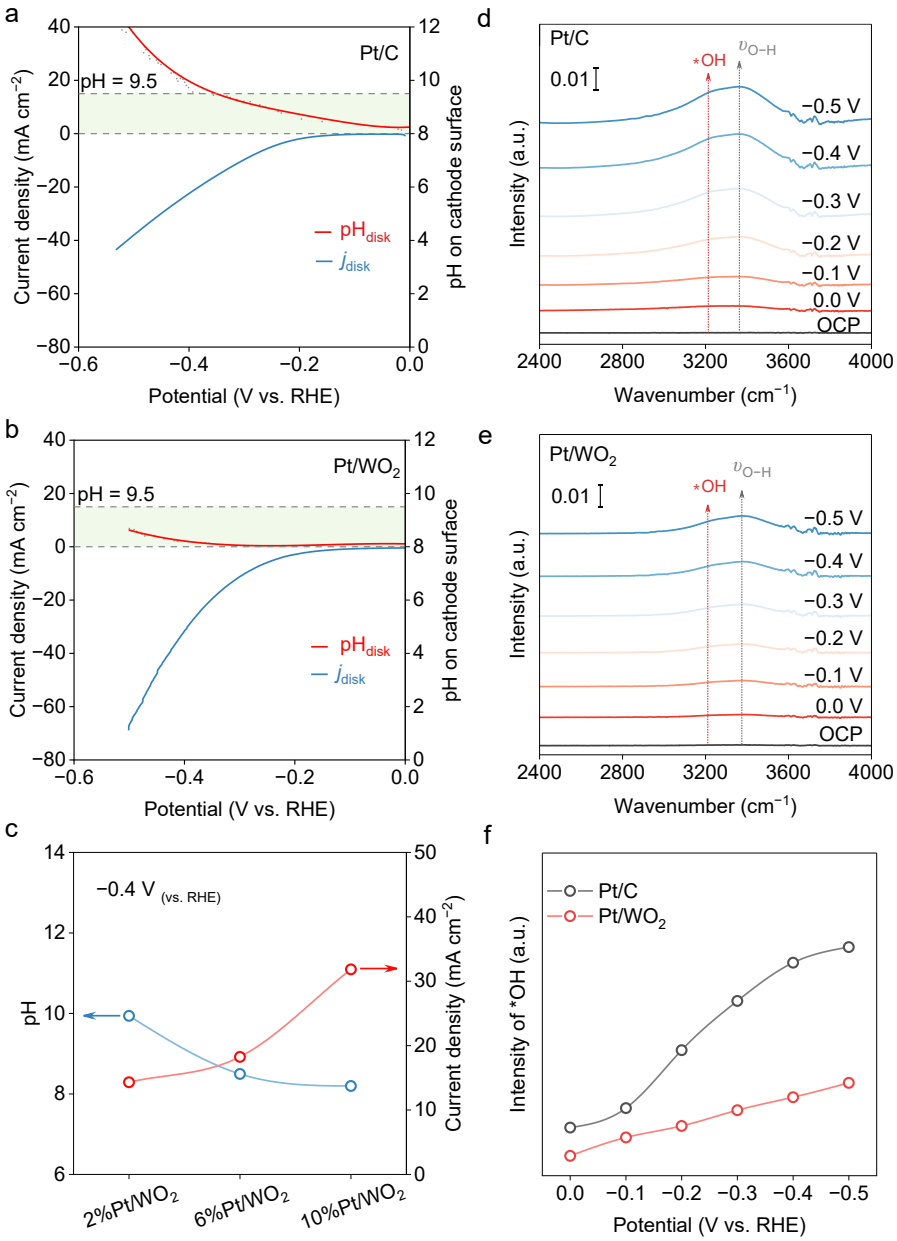


Figure 3. Local pH measurement and investigation on generated OH^-. Local pH on (a) Pt/C and (b) Pt/WO_2 surface in natural seawater under H_2 saturation. (c) Local pH value and corresponding current density over different catalysts at −0.4 V_{RHE}. *In-situ* ATR-IR spectra for (d) Pt/C and (e) Pt/WO_2 at different potential in simulated seawater, respectively. (f) *OH intensity at varying applied potential with Pt/C and Pt/WO_2 catalysts.

on the catalyst surface declines and corresponding current density promotes (**Figure 3c**, S14), evidencing that lower local pH on catalyst surface is favor to HER. To establish the difference in locally generated OH^- on the two catalysts, *in-situ* attenuated total reflectance infrared (ATR-IR) spectroscopy was determined, in which the broad bands boosted with potential at 3240 and 3400 cm^{-1} were assigned to the OH stretching (ν_{O-H}) mode and adsorbed water on catalyst surface, respectively.[42, 43] As seen in **Figure 3d-f**, the absorbed OH (*OH) intensity for Pt/C sample increased with potential more rapidly than that for Pt/WO_2, evidencing high OH^- concentration over Pt/C surface, a finding is consistent with electrochemically local pH findings.

2.4. Dynamic Creation of Local-acid Environment. To establish the origin of local acid-like behavior, the electrochemical behavior of bare WO_2 was determined. Cyclic voltammetry (CV) findings exhibited a hydrogen insertion/extraction redox behavior in natural seawater to evidence the formation of hydrogen tungsten bronze (H_xWO_y) species (**Figure 4a**).[44, 45] A redox peak shift at selected scan rates exhibited a 'slow' response of current to applied potential,[46] evidencing that WO_2 acts as a proton 'sponge' for proton donation and regeneration of active sites (**Figure 4b**). Additionally, *in-situ* Raman spectra for WO_2 evidenced two peaks at 287 and 782 cm^{-1} with increasing external potential, which were in agreement with δ(W–O–W) and

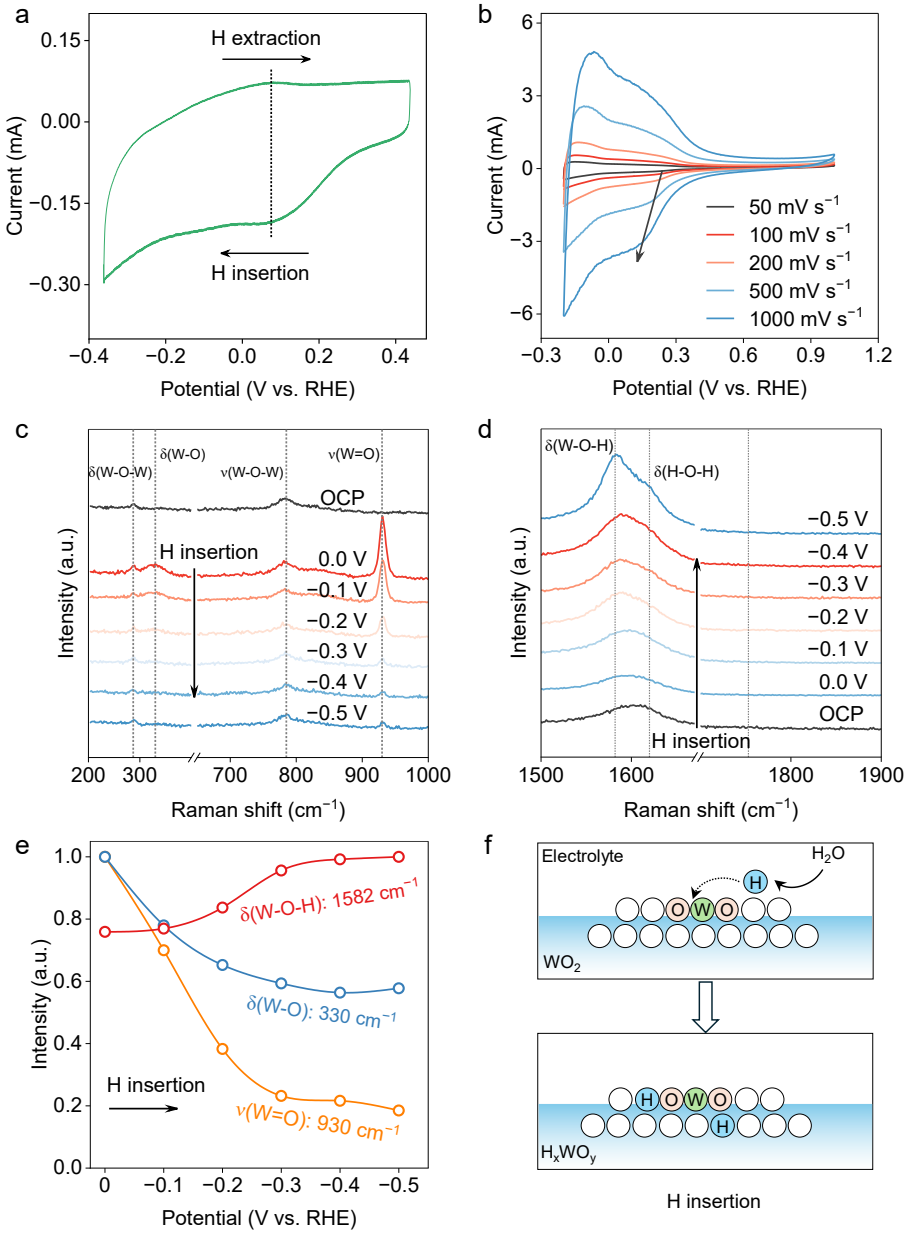


Figure 4. Mechanism for *in-situ* generated proton sponge (H_xWO_y). (a) CV curve for WO_2 from −0.4 to 0.4 V_{RHE} at a scan rate 100 mV s^{-1} in natural seawater under Ar saturation. (b) CV curves for WO_2 in 0.5 M H_2SO_4 under Ar saturation at differing scan rates. (c, d) *In-situ* Raman spectra in simulated seawater for WO_2 at differing potential and (e) correspondingly normalized intensity for δ(W–O–H), δ(W–O) and *ν*(W=O) signals at differing potential. (f) Schematic for *in-situ* dynamic generation of H_xWO_y.

ν(W–O–W) signals for bare WO_2 (**Figure 4c and 1c**).[47,48] Thus, those peak intensities presented no change during reaction (Figure S15). Raman signals at 330 and 930 cm^{-1} were exhibited at 0 V_{RHE} that are attributed to bending vibrations of δ(W–O) bond and ν(W=O) stretching modes of the terminal oxygen, respectively.[23,49] The intensities of these peaks weaken with increasing applied cathodic potential. However, Raman peak for δ(W–O–H) located at 1582 cm^{-1} became apparent and stronger with increasing potential (**Figure 4d**). The increase for δ(W–O–H) peak intensity accompanies by the decrease of δ(W–O) and ν(W=O) peak intensities uncovered the dynamic hydrogen insertion process of WO_2 towards H_xWO_y formation (**Figure 4e** and S15).[50] Under a negative potential therefore, WO_2 acts as active sites for the adsorption and cleavage of H_2O molecules, and hydrogen then inserts into WO_2 and is positioned on an interstitial lattice site to *in-situ* generate H_xWO_y intermediates that serve as a proton storage and electron reservoir (**Figure 4f**). Importantly, this dynamic generation of H_xWO_y is sustainable with a continuous supply of H_2O molecules to WO_2 during reduction reactions.

In-situ Raman spectra for Pt/WO_2 were determined in the range of 1500 to 1900 cm^{-1}. Significantly, the representative peak for H_xWO_y (1582 cm^{-1}) was exhibited, together with a strong signal for H_3O^+ (1750 cm^{-1}) (**Figure 5a left**).[16] In contrast, only two peaks for G band of carbon

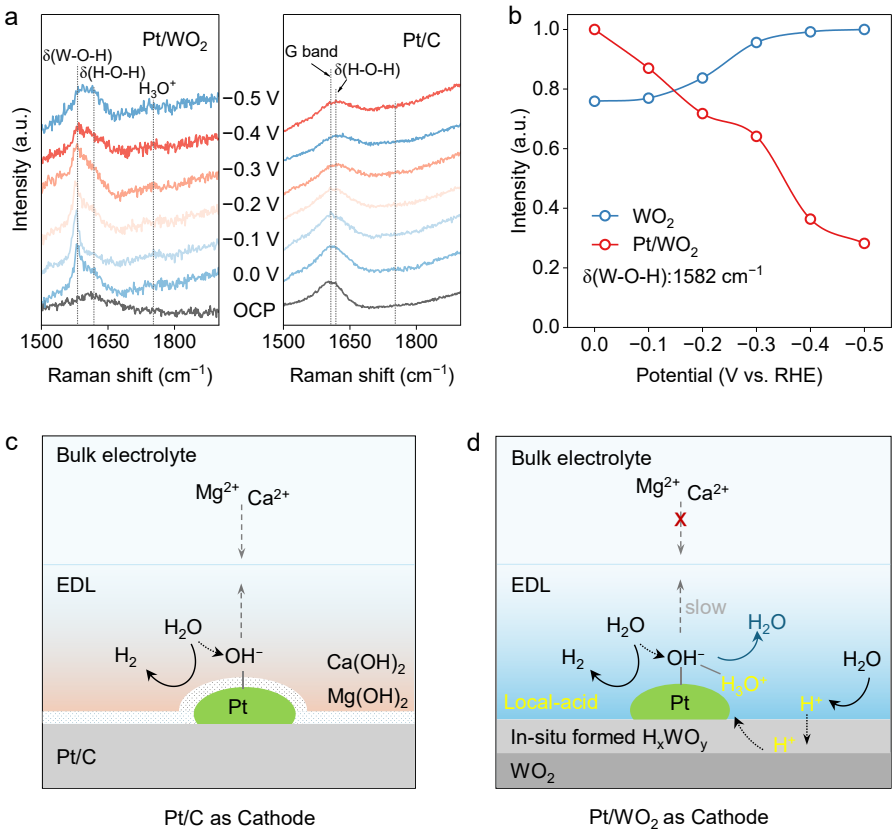


Figure 5. The local acid-like environment. (a) *In-situ* Raman spectra in simulated seawater for Pt/WO_2 and Pt/C and (b) corresponding normalized intensity for δ(W–O–H) signals at differing potential. Schematic for HER mechanism on (c) Pt/C and (d) Pt/WO_2.

and δ(H–O–H) band for interfacial water were exhibited in the Raman spectra for Pt/C (**Figure 5a right**). It can be concluded therefore that a local acid-like environment was created on the Pt/WO_2 surface in natural seawater. The characteristic peak for H_xWO_y (1582 cm^{-1}) over WO_2 and Pt/WO_2 was compared, the nominated peak intensity for WO_2 ran counter to that for Pt/WO_2 (**Figure 5b**). This finding means that the H_xWO_y donates protons to Pt sites for hydrogen formation, namely that, Pt sites tailored on WO_2 facilitate the deprotonation kinetics for *in-situ* generated H_xWO_y.

A mechanism for HER on Pt/C and Pt/WO_2 was therefore hypothesized. In natural seawater electrolysis, for Pt/C, water dissociation commences on the Pt surface producing H^+ and OH^-, the H^+ then couple for HER. The OH^- concentrate on the Pt surface and generate precipitation ($Mg(OH)_2$ and $Ca(OH)_2$), resulting in activity decay (**Figure 5c**). However, for Pt/WO_2, the proton sponge of H_xWO_y is *in-situ* formed under negative potential. The H^+ in proton sponge transfers to Pt and aggregates on Pt surface. Significant number of H_3O^+ create a local acid-like environment that boosts HER in natural seawater and neutralizes concentrated OH^- derived from HER to form water (**Figure 5d**). This process reduces the local pH of Pt/WO_2 together with suppressing precipitation.

2.5. Asymmetric Electrolyzer Performance. To assess application of the local acid-like environment for direct seawater electrolysis, an asymmetric electrolyzer was designed in which natural seawater and freshwater were fed into cathode and anode chambers, respectively (**Figure 6a**). This electrolyzer was assembled with Pt/WO_2 as cathode, NiFe-LDH as anode, and a proton exchange membrane was clamped into the cathode and anode (Figure S16 and S17). This intentional design aims to prevent the penetration of Cl^- ions to the anode chamber, thereby mitigating the attack of Cl^- to anode. Additionally, it enhances conductivity through Na^+ ions to facilitate direct seawater electrolysis.[51, 52] To confirm the asymmetric electrolyzer, a flow-type cell with working area of 1.0 cm^{-2} was fabricated to determine performance with natural seawater electrolysis. When using natural seawater as cathode electrolyte and NaOH solution as anode electrolyte, the flow cell required a voltage of 2.7 V to reach a current density 0.3 A cm^{-2} during an operation of over 100 h test at 70 °C (Figure S18). Importantly, operation voltage is superior to reported natural seawater electrolysis (Table S2).[53-55]

A flow-type electrolyzer with a larger working area of 4.0 cm^{-2} was fabricated to assess performance (Figure S19). As is seen in **Figure 6b**, Pt/C and IrO_2 paired catalysts at 25 °C exhibits a current density of 0.1 A cm^{-2} at cell voltage 5.0 V. This current density is exhibited at 2.5 V *via* replacing IrO_2 to NiFe-LDH. Cell voltage decreases to 1.8 V with Pt/WO_2 as cathode. Significantly, just 3.0 V is required to exhibit 0.5 A cm^{-2} at 25 °C. Optical photographs of Pt/C electrodes confirmed precipitates (compared with that for Pt/WO_2 electrode) following *I-V* test, leading to low

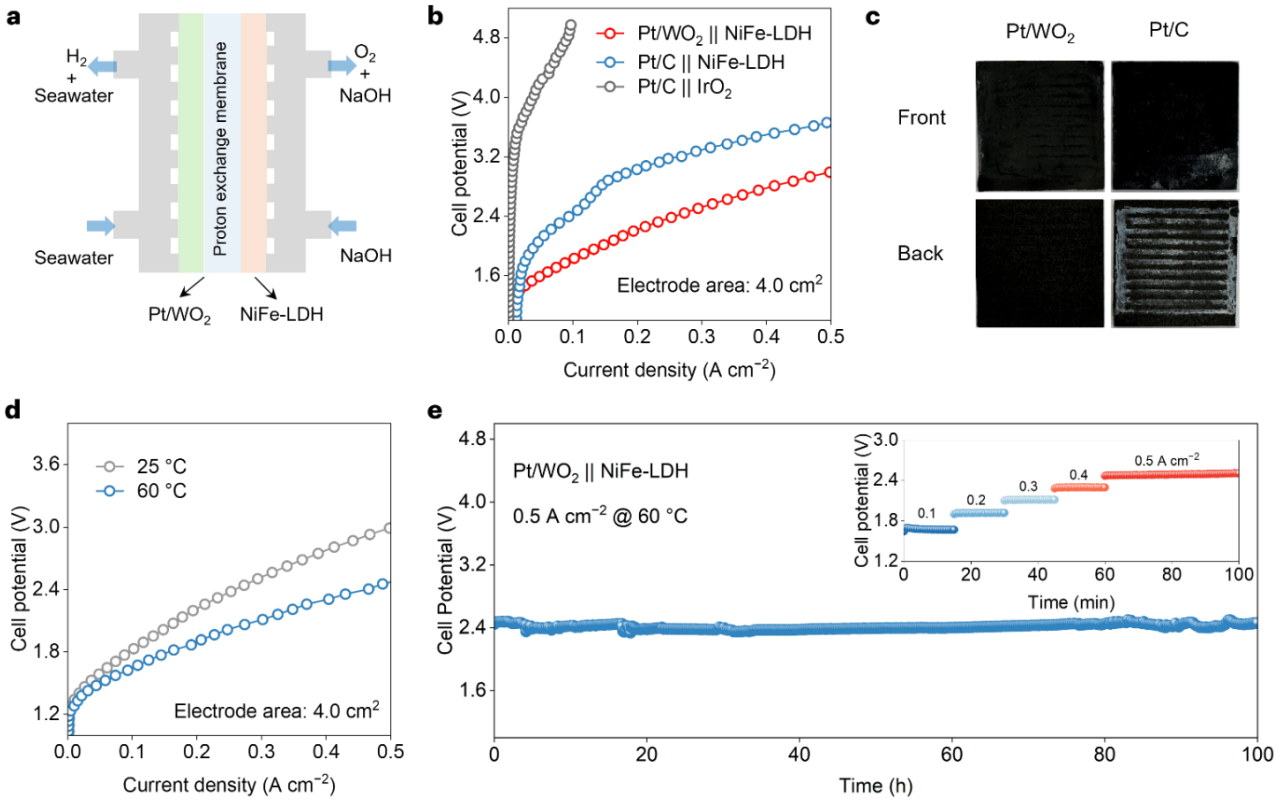


Figure 6. Asymmetric electrolyzer. (a) Schematic diagram of the asymmetric electrolyzer. (b) *I-V* curves for electrolyzer assembled with different catalyst at 25 °C. (c) Optical photograph of cathode electrodes following *I-V* test at 25 °C for Pt/WO_2 and Pt/C. (d) *I-V* curves for electrolyzer assembled with Pt/WO_2 as cathode and NiFe-LDH as anode at 25 and 60 °C. (e) Long-term stability test at 0.5 A cm^{-2} operated at 60 °C, inset is stepped chronopotentiometry tests at differing current density.

performance in natural seawater as catholyte (**Figure 6c**). Additionally, the cell voltage further decreases with increasing temperature to 60 °C; *viz.* a current density of 0.5 A cm^{-2} was exhibited at a cell voltage of 2.47 V (**Figure 6d**). The electrolyzer based on Pt/WO_2 as cathode operated stably at differing current density and continued electrolyzing 100 h at 0.5 A cm^{-2} in natural seawater (**Figure 6e and insert**). Finally, photographs of Pt/WO_2 electrode demonstrated the absence of precipitates on electrode surface after a long stability test (Figure S20).

3. CONCLUSIONS

In summary, a local acid-like environment was developed to eliminate the precipitation and an asymmetric electrolyzer was adopted to circumvent the corrosion problems for natural seawater electrolysis. *In-situ* spectroscopy measurements and controlled electrochemical tests confirmed the local acid-like environment on Pt, created *via* hydrogen insertion of WO_2 during HER. Importantly, this *in-situ* formed environment significantly boosted HER and dynamically neutralized *in-situ* generated OH^- at the cathode surface to suppress precipitation. A long-term stability of > 500 h at 100 mA cm^{-2} was exhibited with natural seawater. An asymmetric electrolyzer fabricated to obviate corrosion exhibited a continuous test in natural seawater for 100 h at a current density of 500 mA cm^{-2} at 60 °C. It is concluded that untreated seawater electrolysis can therefore be used to obviate reliance on strong alkaline or acidic addition(s).

ASSOCIATED CONTENT

Supporting Information

This Supporting Information is available free of charge via the Internet at http://pubs.acs.org.

Experimental methods; structure characterizations of samples such as XRD patterns, SEM images and the corresponding EDS mapping images, TEM images and XPS spectra; electrochemical measurements and so on (PDF)

AUTHOR INFORMATION

Corresponding Author

Yao Zheng – School of Chemical Engineering, The University of Adelaide, Adelaide, SA 5005, Australia; orcid.org/0000-0002-2411-8041;

Email: yao.zheng01@adelaide.edu.au

Shi-Zhang Qiao – School of Chemical Engineering, The University of Adelaide, Adelaide, SA 5005, Australia; orcid.org/0000-0002-4568-8422;

Email: s.qiao@adelaide.edu.au

Authors

Deyu Bao – School of Chemical Engineering, The University of Adelaide, Adelaide, SA 5005, Australia

Linsen Huang – School of Chemical Engineering, The University of Adelaide, Adelaide, SA 5005, Australia

Yingjie Gao – School of Chemical Engineering, The University of Adelaide, Adelaide, SA 5005, Australia

Kenneth Davey – School of Chemical Engineering, The University of Adelaide, Adelaide, SA 5005, Australia

ACKNOWLEDGMENT

The authors gratefully acknowledge financial support provided by the Australian Research Council (CE230100032, DP230102027, DP240102575 and FT200100062).

REFERENCES

(1) Liu, J.; Duan, S.; Shi, H.; Wang, T.; Yang, X.; Huang, Y.; Wu, G.; Li, Q. Rationally designing efficient electrocatalysts for direct seawater splitting: challenges, achievements, and promises. *Angew. Chem. Int. Ed.* **2022**, *61* (45), e202210753.

(2) Logan, B. E.; Shi, L.; Rossi, R. Enabling the use of seawater for hydrogen gas production in water electrolyzers. *Joule* **2021**, *5* (4), 760-762.

(3) Xie, H.; Zhao, Z.; Liu, T.; Wu, Y.; Lan, C.; Jiang, W.; Zhu, L.; Wang, Y.; Yang, D.; Shao, Z. A membrane-based seawater electrolyser for hydrogen generation. *Nature* **2022**, *612* (7941), 673-678.

(4) Hausmann, J. N.; Schlögl, R.; Menezes, P. W.; Driess, M. Is direct seawater splitting economically meaningful? *Energy Environ. Sci.* **2021**, *14* (7), 3679-3685.

(5) Jin, H.; Xu, J.; Liu, H.; Shen, H.; Yu, H.; Jaroniec, M.; Zheng, Y.; Qiao, S.-Z. Emerging materials and technologies for electrocatalytic seawater splitting. *Sci. Adv.* **2023**, *9* (42), eadi7755.

(6) Dresp, S.; Dionigi, F.; Klingenhof, M.; Strasser, P. Direct electrolytic splitting of seawater: opportunities and challenges. *ACS Energy Lett.* **2019**, *4* (4), 933-942.

(7) Karagiannis, I. C.; Soldatos, P. G. Water desalination cost literature: review and assessment. *Desalination* **2008**, *223* (1), 448-456.

(8) Dresp, S.; Dionigi, F.; Loos, S.; Ferreira de Araujo, J.; Spöri, C.; Gliech, M.; Dau, H.; Strasser, P. Direct electrolytic splitting of seawater: activity, selectivity, degradation, and recovery studied from the molecular catalyst structure to the electrolyzer cell level. *Adv. Energy Mater.* **2018**, *8* (22), 1800338.

(9) Nie, N.; Zhang, D.; Wang, Z.; Ge, S.; Gu, Y.; Yang, B.; Lai, J.; Wang, L. Stable p-block metals electronic perturbation in PtM@CNT (M=Ga, In, Pb and Bi) for acidic seawater hydrogen production at commercial current densities. *Appl. Catal. B: Environ.* **2023**, *322*, 122100.

(10) d'Amore-Domenech, R.; Leo, T. J. Sustainable hydrogen production from offshore marine renewable farms: techno-energetic insight on seawater electrolysis technologies. *ACS Sustain. Chem. Eng.* **2019**, *7* (9), 8006-8022.

(11) Tong, W.; Forster, M.; Dionigi, F.; Dresp, S.; Sadeghi Erami, R.; Strasser, P.; Cowan, A. J.; Farràs, P. Electrolysis of low-grade and saline surface water. *Nat. Energy* **2020**, *5* (5), 367-377.

(12) Bennett, J. E. Electrodes for generation of hydrogen and oxygen from seawater. *Int. J. Hydrogen Energy* **1980**, *5* (4), 401-408.

(13) LEDAS, D. W. K. a. A. E. Precipitate formation during sea water electrolysis. *Int. J. Hydrogen Energy* **1982**, *7* (12), 925-932.

(14) Kapp, E. M. The precipitation of calcium and magnesium from sea water by sodium hydroxide. *Biol. Bull.* **1928**, *55* (6), 453-458.

(15) Wang, X.; Jiao, Y.; Li, L.; Zheng, Y.; Qiao, S.-Z. Local environment determined reactant adsorption configuration for enhanced electrocatalytic acetone hydrogenation to propane. *Angew. Chem. Int. Ed.* **2022**, *61* (5), e202114253.

(16) Wang, X.; Xu, C.; Jaroniec, M.; Zheng, Y.; Qiao, S.-Z. Anomalous hydrogen evolution behavior in high-pH environment induced by locally generated hydronium ions. *Nat. Commun.* **2019**, *10* (1), 4876.

(17) Guo, J.; Zheng, Y.; Hu, Z.; Zheng, C.; Mao, J.; Du, K.; Jaroniec, M.; Qiao, S.-Z.; Ling, T. Direct seawater electrolysis by adjusting the local reaction environment of a catalyst. *Nat. Energy* **2023**, *8* (3), 264-272.

(18) Hu, H.; Zhang, Z.; Liu, L.; Che, X.; Wang, J.; Zhu, Y.; Attfield, J. P.; Yang, M. Efficient and durable seawater electrolysis with a V_2O_3-protected catalyst. *Sci. Adv.* **2024**, *10* (20), eadn7012.

(19) Lu, X.; Pan, J.; Lovell, E.; Tan, T. H.; Ng, Y. H.; Amal, R. A sea-change: manganese doped nickel/nickel oxide electrocatalysts for hydrogen generation from seawater. *Energy Environ. Sci.* **2018**, *11* (7), 1898-1910.

(20) Zhu, W.; Wei, Z.; Ma, Y.; Ren, M.; Fu, X.; Li, M.; Zhang, C.; Wang, J.; Guo, S. Energy-efficient electrosynthesis of high value-added active chlorine coupled with H_2 generation from direct seawater electrolysis through decoupling electrolytes. *Angew. Chem. Int. Ed.* **2024**, *136* (15), e202319798.

(21) Tan, H.; Tang, B.; Lu, Y.; Ji, Q.; Lv, L.; Duan, H.; Li, N.; Wang, Y.; Feng, S.; Li, Z.; et al. Engineering a local acid-like environment in alkaline medium for efficient hydrogen evolution reaction. *Nat. Commun.* **2022**, *13* (1), 2024.

(22) Wan, C.; Zhang, Z.; Dong, J.; Xu, M.; Pu, H.; Baumann, D.; Lin, Z.; Wang, S.; Huang, J.; Shah, A. H.; et al. Amorphous nickel hydroxide shell tailors local chemical environment on platinum surface for alkaline hydrogen evolution reaction. *Nat. Mater.* **2023**, *22* (8), 1022–1029.

(23) Zheng, X.; Shi, X.; Ning, H.; Yang, R.; Lu, B.; Luo, Q.; Mao, S.; Xi, L.; Wang, Y. Tailoring a local acid-like microenvironment for efficient neutral hydrogen evolution. *Nat. Commun.* **2023**, *14* (1), 4209.

(24) Li, A.-Z.; Yuan, B.-J.; Xu, M.; Wang, Y.; Zhang, C.; Wang, X.; Wang, X.; Li, J.; Zheng, L.; Li, B.-J.; et al. One-step electrochemical ethylene-to-ethylene glycol conversion over a multitasking molecular catalyst. *J. Am. Chem. Soc.* **2024**, *146* (8), 5622-5633.

(25) Jiang, K.; Liu, B.; Luo, M.; Ning, S.; Peng, M.; Zhao, Y.; Lu, Y.-R.; Chan, T.-S.; De Groot, F. M. F.; Tan, Y. Single platinum atoms embedded in nanoporous cobalt selenide as electrocatalyst for accelerating hydrogen evolution reaction. *Nat. Commun.* **2019**, *10* (1), 1743.

(26) Wang, X.; Zhao, L.; Li, X.; Liu, Y.; Wang, Y.; Yao, Q.; Xie, J.; Xue, Q.; Yan, Z.; Yuan, X.; et al. Atomic-precision Pt_6 nanoclusters for enhanced hydrogen electro-oxidation. *Nat. Commun.* **2022**, *13* (1), 1596.

(27) Qin, R.; Liu, K.; Wu, Q.; Zheng, N. Surface coordination chemistry of atomically dispersed metal catalysts. *Chem. Rev.* **2020**, *120* (21), 11810-11899.

(28) Liu, N.; Xu, M.; Yang, Y.; Zhang, S.; Zhang, J.; Wang, W.; Zheng, L.; Hong, S.; Wei, M. $Au^{\delta-}$–O_v–Ti^{3+} interfacial site: catalytic active center toward low-temperature water gas shift reaction. *ACS Catal.* **2019**, *9* (4), 2707-2717.

(29) Kobayashi, D.; Kobayashi, H.; Wu, D.; Okazoe, S.; Kusada, K.; Yamamoto, T.; Toriyama, T.; Matsumura, S.; Kawaguchi, S.; Kubota, Y.; et al. Significant enhancement of hydrogen evolution reaction activity by negatively charged Pt through light doping of W. *J. Am. Chem. Soc.* **2020**, *142* (41), 17250-17254.

(30) Xu, M.; He, S.; Chen, H.; Cui, G.; Zheng, L.; Wang, B.; Wei, M. TiO_{2-x}-modified Ni nanocatalyst with tunable metal–support interaction for water–gas shift reaction. *ACS Catal.* **2017**, *7* (11), 7600-7609.

(31) Yoshida, H.; Nonoyama, S.; Yazawa, Y.; Hattori, T. Quantitative determination of platinum oxidation state by XANES analysis. *Phys. Scr.* **2005**, *2005* (T115), 813.

(32) Chen, H.; Yu, J.; Liu, L.; Gao, R.-T.; Gao, Z.; Yang, Y.; Chen, Z.; Zhan, S.; Liu, X.; Zhang, X.; et al. Modulating Pt-N/O bonds on Co-doped WO_3 for acid electrocatalytic hydrogen evolution with over 2000 h operation. *Adv. Energy Mater.* **2024**, *14* (19), 2303635.

(33) Chen, G.; Chen, W.; Lu, R.; Ma, C.; Zhang, Z.; Huang, Z.; Weng, J.; Wang, Z.; Han, Y.; Huang, W. Near-atomic-scale superfine alloy clusters for ultrastable acidic hydrogen electrocatalysis. *J. Am. Chem. Soc.* **2023**, *145* (40), 22069-22078.

(34) Xi, G.; Ouyang, S.; Li, P.; Ye, J.; Ma, Q.; Su, N.; Bai, H.; Wang, C. Ultrathin $W_{18}O_{49}$ nanowires with diameters below 1 nm: synthesis, near-infrared absorption, photoluminescence, and photochemical reduction of carbon dioxide. *Angew. Chem. Int. Ed.* **2012**, *51* (10), 2395-2399.

(35) Wu, R.; Zhang, J.; Shi, Y.; Liu, D.; Zhang, B. Metallic WO_2–carbon mesoporous banowires as highly efficient electrocatalysts for hydrogen evolution reaction. *J. Am. Chem. Soc.* **2015**, *137* (22), 6983-6986.

(36) Besnardiere, J.; Ma, B.; Torres-Pardo, A.; Wallez, G.; Kabbour, H.; González-Calbet, J. M.; Von Bardeleben, H. J.; Fleury, B.; Buissette, V.; Sanchez, C.; et al. Structure and electrochromism of two-dimensional octahedral molecular sieve h'-WO_3. *Nat. Commun.* **2019**, *10* (1), 327.

(37) Chen, J.; Chen, C.; Qin, M.; Li, B.; Lin, B.; Mao, Q.; Yang, H.; Liu, B.; Wang, Y. Reversible hydrogen spillover in Ru-WO_{3-x} enhances hydrogen evolution activity in neutral pH water splitting. *Nat. Commun.* **2022**, *13* (1), 5382.

(38) Kim, H.-S.; Cook, J. B.; Lin, H.; Ko, Jesse S.; Tolbert, Sarah H.; Ozolins, V.; Dunn, B. Oxygen vacancies enhance pseudocapacitive charge storage properties of MoO_{3-x}. *Nat. Mater.* **2017**, *16* (4), 454-460.

(39) Jin, H.; Liu, X.; Vasileff, A.; Jiao, Y.; Zhao, Y.; Zheng, Y.; Qiao, S.-Z. Single-crystal nitrogen-rich two-dimensional Mo_5N_6 nanosheets for efficient and stable seawater splitting. *ACS Nano* **2018**, *12* (12), 12761-12769.

(40) Yokoyama, Y.; Miyazaki, K.; Miyahara, Y.; Fukutsuka, T.; Abe, T. In situ measurement of local pH at working electrodes in neutral pH solutions by the rotating ring-disk electrode technique. *ChemElectroChem* **2019**, *6* (18), 4750-4756.

(41) Yokoyama, Y.; Miyazaki, K.; Kondo, Y.; Miyahara, Y.; Fukutsuka, T.; Abe, T. In situ local pH measurements with hydrated iridium oxide ring electrodes in neutral pH aqueous solutions. *Chem. Lett.* **2020**, *49* (2), 195-198.

(42) Kitano, S.; Noguchi, T. G.; Nishihara, M.; Kamitani, K.; Sugiyama, T.; Yoshioka, S.; Miwa, T.; Yoshizawa, K.; Staykov, A.; Yamauchi, M. Heterointerface created on Au-cluster-loaded unilamellar hydroxide electrocatalysts as a highly active site for the oxygen evolution reaction. *Adv. Mater.* **2022**, *34* (16), 2110552.

(43) Yang, X.; Nash, J.; Oliveira, N.; Yan, Y.; Xu, B. Understanding the pH dependence of underpotential deposited hydrogen on platinum. *Angew. Chem. Int. Ed.* **2019**, *58* (49), 17718-17723.

(44) Park, J.; Lee, S.; Kim, H.-E.; Cho, A.; Kim, S.; Ye, Y.; Han, J. W.; Lee, H.; Jang, J. H.; Lee, J. Investigation of the support effect in atomically dispersed Pt on WO_{3-x} for utilization of Pt in the hydrogen evolution reaction. *Angew. Chem. Int. Ed.* **2019**, *58* (45), 16038-16042.

(45) Zheng, H.; Ou, J. Z.; Strano, M. S.; Kaner, R. B.; Mitchell, A.; Kalantar-zadeh, K. Nanostructured tungsten oxide – properties, synthesis, and applications. *Adv. Funct. Mater.* **2011**, *21* (12), 2175-2196.

(46) Jiang, H.; Hong, J. J.; Wu, X.; Surta, T. W.; Qi, Y.; Dong, S.; Li, Z.; Leonard, D. P.; Holoubek, J. J.; Wong, J. C.; et al. Insights on the proton insertion mechanism in the electrode of hexagonal tungsten oxide hydrate. *J. Am. Chem. Soc.* **2018**, *140* (37), 11556-11559.

(47) Frey, G. L.; Rothschild, A.; Sloan, J.; Rosentsveig, R.; Popovitz-Biro, R.; Tenne, R. Investigations of nonstoichiometric tungsten oxide nanoparticles. *J. Solid State Chem.* **2001**, *162* (2), 300-314.

(48) Lyu, C.; Zhang, L.; Zhang, X.; Zhang, H.; Xie, H.; Zhang, J.; Liu, Y.; Liu, Y.; Wu, R.; Zhang, J.; et al. Controlled synthesis of sub-millimeter nonlayered WO_2 nanoplates via a WSe_2-assisted method. *Adv. Mater.* **2023**, *35* (12), 2207895.

(49) Gabrusenoks, J. V.; Cikmach, P. D.; Lusis, A. R.; Kleperis, J. J.; Ramans, G. M. Electrochromic colour centres in amorphous tungsten trioxide thin films. *Solid State Ionics* **1984**, *14* (1), 25-30.

(50) Lee, S.-H.; Cheong, H. M.; Tracy, C. E.; Mascarenhas, A.; Benson, D. K.; Deb, S. K. Raman spectroscopic studies of electrochromic a-WO_3. *Electrochim. Acta* **1999**, *44* (18), 3111-3115.

(51) Dresp, S.; Ngo Thanh, T.; Klingenhof, M.; Brückner, S.; Hauke, P.; Strasser, P. Efficient direct seawater electrolysers using selective alkaline NiFe-LDH as OER catalyst in asymmetric electrolyte feeds. *Energy Environ. Sci.* **2020**, *13* (6), 1725-1729.

(52) A sodium-ion-conducted asymmetric electrolyzer to lower the operation voltage for direct seawater electrolysis. *Nat. Commun.* **2023**, *14* (1), 3934.

(53) Zhao, Y.; Jin, B.; Zheng, Y.; Jin, H.; Jiao, Y.; Qiao, S. Z. Charge state manipulation of cobalt selenide catalyst for overall seawater electrolysis. *Adv. Energy Mater.* **2018**, *8* (29), 1801926.

(54) Yu, L.; Wu, L.; Song, S.; Mcelhenny, B.; Zhang, F.; Chen, S.; Ren, Z. Hydrogen generation from seawater electrolysis over a sandwich-like NiCoN|Ni_xP|NiCoN microsheet array catalyst. *ACS Energy Lett.* **2020**, *5* (8), 2681-2689.

(55) Yu, L.; Zhu, Q.; Song, S.; McElhenny, B.; Wang, D.; Wu, C.; Qin, Z.; Bao, J.; Yu, Y.; Chen, S.; et al. Non-noble metal-nitride based electrocatalysts for high-performance alkaline seawater electrolysis. *Nat. Commun.* **2019**, *10* (1), 5106.

For Table of Contents Only

